Module Technology for Agrivoltaics: Vertical Bifacial Versus Tilted Monofacial Farms

Muhammad Hussnain Riaz, Hassan Imran, *Member, IEEE*, Rehan Younas, Muhammad Ashraful Alam, *Fellow, IEEE*, and Nauman Zafar Butt, *Member, IEEE*

***Abstract*—Agrivoltaics (AV) is an innovative approach in which solar photovoltaic (PV) energy generation is collocated with agricultural production to enable food–energy–water synergies and landscape ecological conservation. This dual-use requirement leads to unique cooptimization challenges (*e.g.*, shading, soiling, and spacing) that make module technology and farm topology choices distinctly different from the traditional solar farms. Here, we compare the performance of the traditional optimally titled North/South (*N/S*)-faced monofacial farms with a potential alternative based on vertical East/West (*E/W*)-faced bifacial farms. Remarkably, the vertical farm produces essentially the same energy output and photosynthetically active radiation (*PAR*) compared with the traditional farms as long as the PV array density is reduced to half or lower relative to that for the standard ground-mounted PV farms. Our results explain the relative merits of the traditional monofacial versus vertical bifacial farms as a function of array density, acceptable *PAR* deficit, and energy production. The combined *PAR*/Energy yields for the vertical bifacial farm may not always be superior, it could still be an attractive choice for AV due to its distinct advantages such as minimum land coverage, least hindrance to the farm machinery and rainfall, inherent resilience to PV soiling, easier cleaning, and cost advantages due to the potentially reduced elevation.**

***Index Terms*—Agrivoltaics, bifacial, farm yield, vertical.**

I. Introduction

While the concept of agrivoltaics (AV) dates back to 1980s [1], the dramatic cost reduction of solar modules over the last decade and world-wide proliferation of photovoltaic (PV) technologies have made the approach potentially viable in many parts of the world. This dual approach of harvesting energy and food together in a given land area can maximize the land productivity with additional synergistic benefits including reduced water budget, improved crop yield, agricultural land preservation, and socioeconomic welfare of farmers [2]–[9]. The AV farming can offer an attractive solution to a potential conflict between rapidly spreading ground-mounted solar PV parks and the agricultural production, landscape ecology, and biodiversity [10], [11]. Moreover, AV can be leveraged to enable crop resilience against the increasing climate change vulnerabilities, such as the excessive heat stress and drought, in particular, for hot and arid climates [5]. Other synergistic benefits may include sharing of water between the cleaning of panels and irrigation to reduce the overall water and maintenance cost.

The AV farm design has so far explored the traditional fixed-tilt North/South (*N/S*)-faced PV arrays or solar tracking schemes with limited focus on comparative analysis between module technologies. The fixed-tilt systems have primarily been explored in two configurations: full and half PV array densities that correspond to row to row pitch being twice and four times the height of the panels, respectively. Dupraz *et al.* [12], [13] predicted that 35–73% increase in the land equivalent ratio *(LER)*, a metric to quantify the land productivity, was possible for Montpelier (43 °N), France, when solar arrays were arranged at full and half densities, respectively. Marrou *et al.* [14] performed AV experiments in Montpelier, France, using full and half density arrays for both short-cycle (lettuce and cucumber) and long-cycle (durum wheat) crops. The study emphasized that the main focus for developing the AV system should be on exploring mitigation strategies for light reduction and optimal selection of crops [11]. Majumdar and Pasqualetti [10] modeled the AV system at Pheonix, AZ, USA, and showed that south-faced solar arrays titled at 30° received 60% and 80% of the total global radiation for half and quarter density of solar arrays, respectively, as compared with an open field. Malu *et al.* [15] modeled AV grape farming for Maharashtra (19.59° N), India, and predicted that it could increase the economic value of the land by 15 times as compared with the conventional farming.

Amaducci *et al.* [16] showed that the reduction of global radiation under *AV* was affected more by panel density than by dynamic management of tilt through solar tracking. Sekiyama and Nagashima [17] did an experiment in Ichihara City (35.37° N, 140.13° W), Japan, using PV arrays at full versus half density and found that the corn yield for the half density remarkably outperformed that of the open (control) farm by 5.6%.

Although the reported studies have successfully demonstrated the potential of *AV* across various climates and crops, the choice of module technology and farm topology have not been explored. Technology innovations to address practical challenges including the need to elevate the panels to 3–5 m, the issue about soiling

Manuscript received August 18, 2020; revised October 24, 2020; accepted December 24, 2020. Date of publication January 21, 2021; date of current version February 19, 2021. *(Muhammad Hussnain Riaz and Hassan Imran contributed equally to this work.) (Corresponding author: Nauman Zafar Butt.)*

Muhammad Hussnain Riaz, Hassan Imran, Rehan Younas, and Nauman Zafar Butt are with the Department of Electrical Engineering, School of Science and Engineering, Lahore University of Management Sciences, Lahore 54792, Pakistan (e-mail: hussnainriaz8@gmail.com; hassan.imran.ee@gmail.com; rehanyounas@gmail.com; nzbutt@gmail.com).

Muhammad Ashraful Alam is with the School of Electrical and Computer Engineering, Purdue University, West Lafayette, IN 47907 USA (e-mail: alam@purdue.edu).

Color versions of one or more figures in this article are available at https://doi.org/10.1109/JPHOTOV.2020.3048225.

Digital Object Identifier 10.1109/JPHOTOV.2020.3048225

and the difficulty to clean at high elevation, etc., have so far not been considered. Among the available module technologies, the potential for bifacial solar panels has not yet been studied in detail although the bifacial PV is attracting a great attraction in the commercial PV market due to higher performance and temperature insensitivity [18]–[20]. In this article, we address these issues by exploring the vertically tilted East/West (*E/W*)-faced bifacial (*bi-E/W*) panels, which can be of great potential interest for AV due to a number of practical advantages including inherent resilience to soiling losses, minimum land coverage that provides least hindrance to the farm machinery and rainfall, and possibility to mount much closer to the ground, hence, offering significantly lower installation cost and easier access for cleaning [21], [22]. The soiling losses can be substantial for tilted panels in many climates in south Asia, middle East, and north Africa, where power losses due to soling in tilted panels could be as high as 1% per day [23]–[25]. Soiling losses are known to mitigate strongly as the panel tilt varies from horizontal to vertical [23]. For this reason, in arid climates where long dry periods (between successive rain events) can exacerbate PV soiling losses and drought concerns for the crops, a vertical panel AV arrangement could be especially advantageous. Despite of these potential attractions, there is no study currently available in literature to explore relative potential for the vertical bifacial AV farming.

In this article, we present a computational investigation into the vertical bifacial AV farms that for the first time explores its relative advantages and tradeoffs as compared with the conventional *N/S*-tilted monofacial and bifacial AV farms. By developing a rigorous model for the radiation interception at the panels and *PAR* transmission to the crops, respectively, we specifically address the following questions when comparing these AV orientations.

1) What are the relative food–energy implications as the PV array density is varied?
2) How does the tilt angle change the relative food–energy production?
3) What land productivities can be achieved relative to the standalone energy and crop systems across the year?

The primary goal here is to establish the comparative performance of vertical AV farms using traditional metrics, *i.e.*, PV energy and *PAR* without considering the complex crop modeling, which is beyond the scope of this article. This approach may be imperfect in terms of evaluating the specific crop yields, but would offer guidance and establish principles of technology assessment.

This article is divided into four sections. In Section II, we describe the detailed methodology. Results are discussed in Section III, whereas Section IV concludes this article.

II. Methodology

For calculating energy harvested by solar modules, we assume that arrays are long enough so that the edge effects are negligible. This allows for solving the PV energy generation in 2D assuming symmetry in the third (infinitely long) dimension parallel to the row. The solar farm consists of solar modules of height (h) that are mounted at an elevation (E) above the ground and the pitch (row-to-row separation) between them is p. The two PV orientations, *i.e.*, *N/S* and *E/W* are illustrated in Fig. 1.

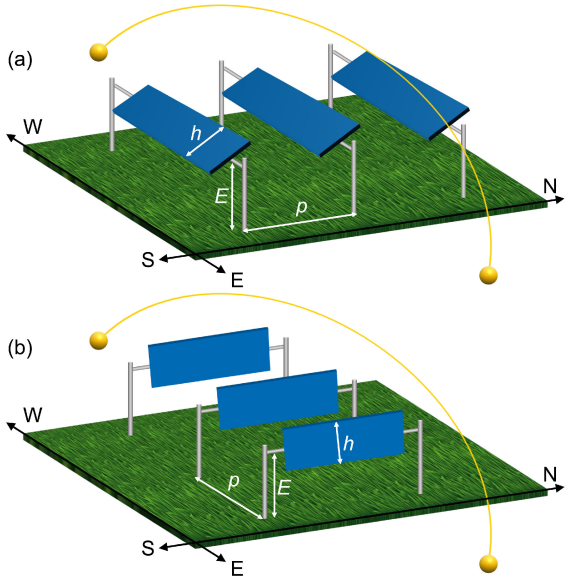

Fig. 1. (a) Tilted monofacial South facing (*mono-N/S*). (b) Vertical bifacial East-west facing (*bi-E/W*) solar modules.

A. Solar Irradiation and PV Models

Recent work presented in [26] provides a detailed modeling approach for solar energy harvested in ground-mounted bifacial PV arrays including the effects of self-/mutual shading. For AV applications, however, PV arrays typically need to be elevated above ground to conveniently allow agricultural operations, hence, necessitating models that work for elevated PV structures. To precisely calculate the shading patterns for the crops and the PV energy generation for elevated panels, we develop new analytical models to calculate the direct/diffused albedo collection by the elevated PV array and the diffused *PAR* transmitted under the panels including the masking by the elevated PV array. Model validation is done by comparison to published experimental data.

1) Calculation of Global Horizontal, Direct, and Diffuse Irradiance: The global horizontal irradiance (I_{global}) and its components, *i.e.*, direct normal (I_{dir}) and diffused horizontal irradiance (I_{diff}) along with the sun's trajectory (defined by zenith (θ_z) and azimuth (γ_s) angles) at any location (latitude and longitude) were calculated using NREL's algorithm [27] implemented in Sandia's photovoltaic modeling library (PVLib) [28]. The Huarwitz clear sky model [29] was used to calculate I_{global} with a 1-min time resolution. Satellite-derived data from NASA Surface Meteorology and Solar Energy database [30] were used to calibrate the location-specific climate factors similar to the approach used in [31]–[33].

2) Calculation of Shadow Lengths: The shadow for the direct beam of the Sun along the pitch is calculated on the ground or at any elevation below the PV array. The shadow length at the ground due to the top and bottom points of the module (denoted

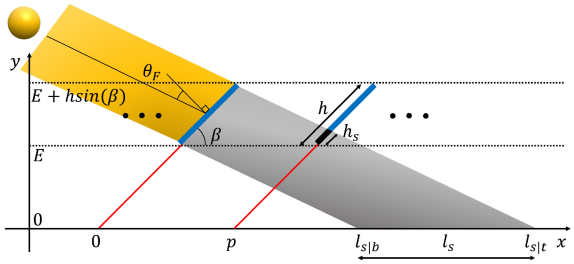

Fig. 2. Illustration of direct sunlight incident on solar modules of height h, tilted at an angle β, and mounted at an elevation E above the ground. The shadow length l_s on the ground and shadow height on the adjacent module h_s along with the angle of incident θ_F are also depicted.

by $l_{s|t}$ and $l_{s|b}$, respectively; see Fig. 2) is given as

$$\left.\begin{aligned} l_{s|t} &= \frac{(E + h\cdot\sin\beta)\cdot\cos\theta_F}{\sin(90-\beta+\theta_F)\cdot\sin\beta} \\ l_{s|b} &= \frac{E\cdot\cos\theta_F}{\sin(90-\beta+\theta_F)\cdot\sin\beta} \end{aligned}\right\} \quad (1)$$

where θ_F is the angle of incidence [26] at the front surface and β is the tilt angle. The actual shadow length (l_s) on the ground is given by $l_s = l_{s|t} - l_{s|b}$. If $l_s > p$, then a part of the shadow with height denoted by h_s will be dropped on the adjacent module (see Fig. 2) causing the mutual shading

$$h_s = \frac{\sin[90+\theta_F-\beta]\times[l_{s|t}-p]}{\sin[90-\theta_F]} - \frac{E}{\sin(\beta)}. \quad (2)$$

The mutual shading between modules becomes significant as *p/h* is reduced.

3) Energy Harvested From Direct and Diffuse Irradiance: The calculation for the direct and diffused radiation intercepted by the elevated panels is identical to that for ground-mounted panels, therefore, the existing modeling approaches described in [26] and [31] are applied. The efficiency of the front/back surfaces of the module under direct and diffused light are taken as 19% and 16%, respectively [31], [34], [35]. The PV power estimate for direct irradiance incorporates the irradiance loss due to mutual shading but ignores the practical cell configuration on modules, which usually involves bypass diodes. The power-output estimate in our model is, therefore, an optimistic upper bound when mutual shading is significant.

4) Energy Harvested From Direct Albedo Irradiance: Fig. 3 shows the ground regions under light (yellow) and shadow (gray) at a certain time during a day. Each point z on the front/back face of a panel receives direct albedo from all of the illuminated (yellow) regions that lie inside its view toward the ground that is not blocked by the adjacent panels [see Fig. 3(b)]. At any given time during the day, the shadow/light pattern on the ground is computed using (1). The view factor for the direct albedo at point z for either the front (F) or the back (B) face of the panel is computed by the angles $\psi^{(i)}_{t|F}$, $\psi^{(i)}_{b|F}$, $\psi^{(i)}_{t|B}$, and $\psi^{(i)}_{b|B}$ subtended by the edges of shadow (gray regions) (*i.e.,* $l_{s|t}$ and $l_{s|b}$) from the ground to the front and back faces of the module, respectively

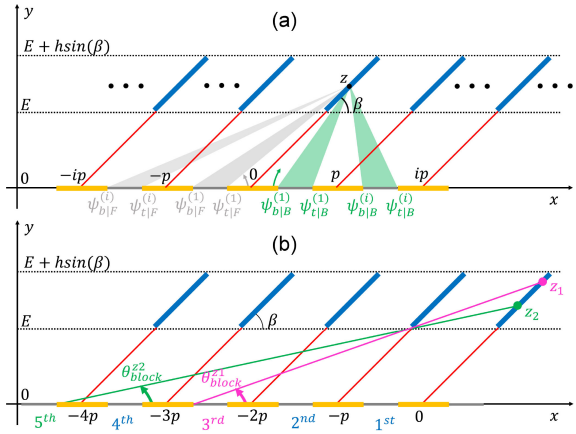

Fig. 3. (a) Angles subtended by the edges of the shade on the ground due to direct irradiance at a given time on the front and back surfaces of the modules. The green and gray arrow represent that angles are measured from the ground in clockwise and anticlockwise directions, respectively. (b) Blocking angles (θ^z_{block}) that determine the limits of view from panel to ground.

[see Fig. 3(a)].

$$\left.\begin{aligned} \psi^{(i)}_{t|F}(z) &= \tan^{-1}\left[\frac{E+z\cdot\sin\beta}{i\times p - l_{s|t} + \frac{E+z\cdot\sin\beta}{\tan\beta}}\right] \\ \psi^{(i)}_{b|F}(z) &= \tan^{-1}\left[\frac{E+z\cdot\sin\beta}{i\times p - l_{s|b} + \frac{E+z\cdot\sin\beta}{\tan\beta}}\right] \\ \psi^{(i)}_{t|B}(z) &= 180^\circ - \tan^{-1}\left[\frac{E+z\cdot\sin\beta}{-(i-1)\times p - l_{s|t} + \frac{E+z\cdot\sin\beta}{\tan\beta}}\right] \\ \psi^{(i)}_{b|B}(z) &= 180^\circ - \tan^{-1}\left[\frac{E+z\cdot\sin\beta}{-(i-1)\times p - l_{s|b} + \frac{E+z\cdot\sin\beta}{\tan\beta}}\right] \end{aligned}\right\}. \quad (3)$$

Small case letters (b,t) represent the shadow edges as shown in Fig. 2. The superscript represents the neighboring pitches adjacent to the panel. For example, $\psi^{(1)}_{b|B}$ represents the angle in the first (adjacent) pitch toward the front face at point z, from the shadow edge that is cast by the bottom of the first (adjacent) panel. The view factor for the front surface of the module from point z to the unshaded part of the ground is computed by summing the contributions of all pitches until $\psi^{(i)}_F$ exceeds θ^z_{block} [as defined in Fig. 3(b)]

$$F_{dz\to Ugnd|F}(z) = \frac{1}{2}\times\begin{cases} \sum_i\left\{\sin\left(\psi^{(i)}_{b|F}\right) - \sin\left(\psi^{(i+1)}_{t|F}\right)\right\} + \\ \sin\beta - \sin\left(\psi^{(i)}_{t|F}\right) \quad ;\tilde{}\text{if}\tilde{}\,\theta_F \le 90^\circ \\ \sum_i\left\{\sin\left(\psi^{(i)}_{t|F}\right) - \sin\left(\psi^{(i+1)}_{b|F}\right)\right\} + \\ \sin\beta - \sin\left(\psi^{(i)}_{b|F}\right) \quad ;\tilde{}\text{if}\tilde{}\,\theta_F > 90^\circ \end{cases}. \quad (4)$$

As θ^z_{block} varies for each point z on the panel, the upper limit of i in (4) is a function of z as illustrated in Fig. 3(b). The view factor for the back surface, $F_{dz\to Ugnd|B}$ can also be computed similar to (4).

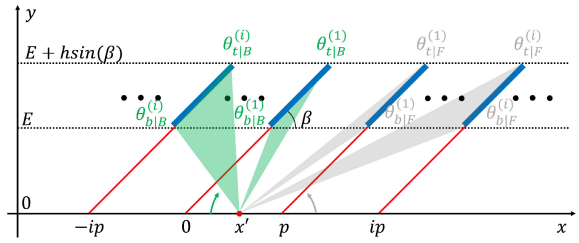

Fig. 4. Masking of diffuse albedo light on the face of the module by the adjacent modules in either directions.

The power received at any point z on the front and back faces of the module due to direct albedo is given by

$$\left.\begin{aligned} I_{\text{M,Alb:dir|F}}(z) &= I_{\text{gnd;dir}} \times \eta_{\text{diff|F}} \times R_{\text{A}} \times F_{\text{d}z\rightarrow\text{Ugnd|F}}(z) \\ I_{\text{M,Alb:dir|B}}(z) &= I_{\text{gnd;dir}} \times \eta_{\text{diff|B}} \times R_{\text{A}} \times F_{\text{d}z\rightarrow\text{Ugnd|B}}(z) \end{aligned}\right\} \tag{5}$$

where $I_{\text{gnd;dir}}$ represents the direct irradiance reaching the ground and R_{A} is the ground albedo and considered equal to 0.25 in all calculations. The total power ($I_{\text{M,Alb:dir}}$) generated by direct albedo per unit solar farm area is then computed by numerically integrating the generated power at each dz along the panel height via the trapezoidal method in MATLAB.

$$I_{\text{M,Alb:dir}} = \frac{1}{p} \times \int_0^h \left[I_{\text{M,Alb:dir|F}}(z) + I_{\text{M,Alb:dir|B}}(z) \right] dz. \tag{6}$$

5) Energy Harvested From Diffuse Albedo Irradiance: For any point x between the two adjacent panels $[0 \le x \le p]$, the masking angles ($\theta^{(i)}_{\text{t|F}}$ and $\theta^{(i)}_{\text{b|F}}$) for the diffused sunlight subtended from x to the top and bottom points of PV modules at the back surfaces (see Fig. 4) are given by

$$\left.\begin{aligned} \theta^{(i)}_{\text{t|B}}(x) &= 180 - \tan^{-1}\left[\frac{E + h\cdot\sin\beta}{(i-1)p - x + \frac{E+h\cdot\sin\beta}{\tan\beta}}\right] \\ \theta^{(i)}_{\text{b|B}}(x) &= 180 - \tan^{-1}\left[\frac{E}{(i-1)p - x + \frac{E}{\tan\beta}}\right] \end{aligned}\right\}. \tag{7}$$

The total masking angle for x for the back side of the panel over the entire farm is given as

$$\Delta\theta_1 = \int_0^p \left[\sum_i \left(\theta^{(i)}_{\text{t|B}} - \theta^{(i)}_{\text{b|B}} \right) \right] dx. \tag{8}$$

Similarly, masking angles for the front side of the panel, *i.e.*, $\theta^{(i)}_{\text{t|F}}$ and $\theta^{(i)}_{\text{b|F}}$ are given as

$$\left.\begin{aligned} \theta^{(i)}_{\text{t|F}}(x) &= \tan^{-1}\left[\frac{E + h\cdot\sin\beta}{(i-1)p - x + \frac{E+h\cdot\sin\beta}{\tan\beta}}\right] \\ \theta^{(i)}_{\text{b|F}}(x) &= \tan^{-1}\left[\frac{E}{(i-1)p - x + \frac{E}{\tan\beta}}\right] \end{aligned}\right\}. \tag{9}$$

The total masking angle for x for the front side of the panel over the entire farm is given as

$$\Delta\theta_2 = \int_0^p \left[\sum_i \left(\theta^{(i)}_{\text{t|F}} - \theta^{(i)}_{\text{b|F}} \right) \right] dx. \tag{10}$$

The average diffused light reaching the ground is given as [31]

$$I_{\text{gnd;diff}} = I_{\text{diff}} \times \frac{1}{2} \left[\cos(\Delta\theta_1) + \cos(\Delta\theta_2) \right]. \tag{11}$$

The power generated by diffuse albedo for any point z by the front and back surfaces of the module is then given by

$$\left.\begin{aligned} I_{\text{M,Alb:diff|F}}(z) &= \eta_{\text{diff|F}} \times I_{\text{gnd;diff}} \times R_{\text{A}} \times F_{\text{d}z\rightarrow\text{gnd|F}} \\ I_{\text{M,Alb:diff|B}}(z) &= \eta_{\text{diff|B}} \times I_{\text{gnd;diff}} \times R_{\text{A}} \times F_{\text{d}z\rightarrow\text{gnd|B}} \end{aligned}\right\} \tag{12}$$

where $F_{\text{d}z\rightarrow\text{gnd|F}}$ and $F_{\text{d}z\rightarrow\text{gnd|B}}$ are view factors at any point z along the module height masked by the front and back surfaces of the module to the ground, respectively [26]. The total power generated ($I_{\text{M,Alb:diff}}$) by the diffused albedo per unit solar farm area is calculated using numerical integration

$$I_{\text{M,Alb:diff}} = \frac{1}{p} \times \int_0^h \left[I_{\text{M,Alb:diff|F}}(z) + I_{\text{M,Alb:diff|B}}(z) \right] dz. \tag{13}$$

The total PV power generated (I_{M}) per unit farm area is then calculated as

$$I_{\text{M}} = I_{\text{M,dir}} + I_{\text{M,diff}} + I_{\text{M,Alb:dir}} + I_{\text{M,Alb:diff}}. \tag{14}$$

B. Transmitted PAR Under the Panels

At any given time, the observation point under the panels along the pitch is either under shade, hence, receiving the diffused light only, $I_{\text{op}} = I_{\text{gnd;diff}}$, or receiving both direct as well as diffused sunlight ($I_{\text{op}} = I_{\text{gnd;dir}} + I_{\text{gnd;diff}}$). The relative cumulative radiation (PAR_r) incident at a specific crop height is calculated as the percentage ratio of the light received under panel coverage to the total incident light with no panels installed

$$\text{PAR}_r(\%) = \frac{1}{k} \sum_{\text{op=1}}^{k} \frac{I_{\text{op}}}{I_{\text{global}}} \times 100\% \tag{15}$$

Here, k is varied to cover the entire region within a pitch.

C. Calculation of the Land Productivity Factor

Typically, the *LER*, a metric that was originally defined for measuring the efficacy of intercropping [4], has been used to characterize the productivity of land for AV relative to the standalone PV systems and agricultural farms. It however requires the estimation of the relative crop yields, which may have a wide variation across different crop species and can have a complex dependence on the dynamically varying shades and other microclimate factors that are beyond the scope of the present work. Here, for the purpose of comparing various module technologies and farm topologies, we define a simpler metric named land productivity factor (*LPF*) a crop independent parameter that estimates the AV land productivity by adding the relative yields for PV energy and the transmitted PAR at the crop level

$$\text{LPF} = \frac{\text{PAR}_r}{100} + \frac{Y_{\text{e}}(\text{AV})}{Y_{\text{e}}(\text{PV})} \tag{16}$$

where $Y_{\text{e}}(\text{AV})$ = energy yield for AV farm;

$Y_{\text{e}}(\text{PV})$ = energy yield for the traditional standalone solar PV system at $p/h \approx 2$ facing N/S at standard fixed tilt.

D. Effect of Temperature and Soiling on PV Energy

To estimate the soiling effect for Lahore, recently published experimental data are used [23], [36], which reports the soiling

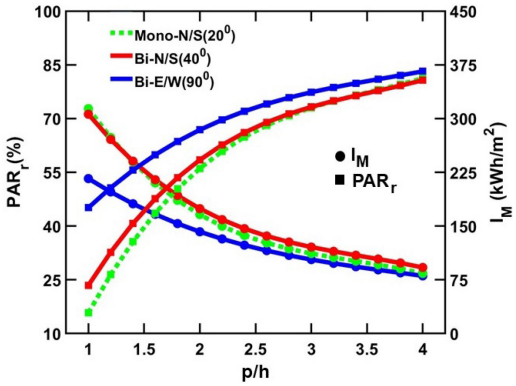

Fig. 5. PAR_r and I_M as a function of *p/h* for *E/W* and *N/S* PV configurations.

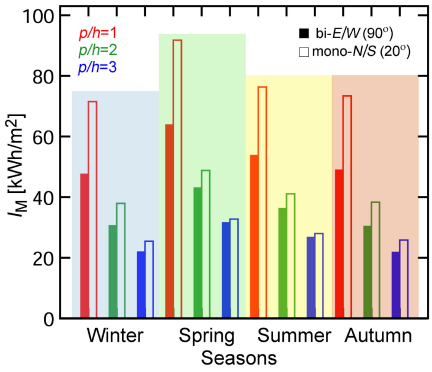

Fig. 6. Energy generated in *bi-E/W* PV, and *mono-N/S* PV farm tilted at $\beta = 20^\circ$ during all months of the year for different values of panel density.

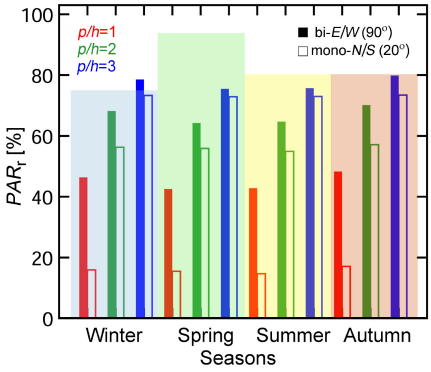

Fig. 7. PAR_r for (a) *bi-E/W* PV, and (b) *mono-N/S* PV farm tilted at $\beta = 20^\circ$ during all months of the year for different values of panel density.

rate of 0.9%/day for the tilt angle of 20°. The relative soiling loss for the vertical tilt is reported to be negligible [23]. Based on this, the power loss due to soiling for *mono-N/S* PV is calculated to be 4–7% higher as compared with *bi-E/W* assuming the cleaning schedules of one week and two weeks, respectively. Although we emphasize the superior soiling performance for the vertical panels, soiling loss is not specifically included in the PV output shown in Section III because of its variability associated with cleaning frequency and the seasonal rainfall patterns.

III. Results and Discussion

The performance of the AV system has been assessed for the *N/S*-tilted and *E/W* vertical PV schemes for Lahore (31.5° N, 74.3° E) for a range of panel density including the standard ($p/h = 2$), half ($p/h = 4$), and double ($p/h = 1$) across all months of the year.

A. PV Energy Generation and the Transmitted PAR

Fig. 5 illustrates the annual PV energy production and PAR_r for the PV schemes under consideration. For low density of panels (*p/h*≈4), mutual shading between the panels is negligible, while the energy production and PAR_r for the PV schemes are relatively similar. As the panel density is increased, a couple of effects become important due to which the PV output and PAR_r for *bi-E/W* significantly diverge as compared with the *N/S*-tilted schemes. First, the mutual shading between the panels starts to increase dominantly for bi-E/W, which lowers its relative PV energy yield while simultaneously increasing the PAR_r. This effect is stronger for *bi-E/W* due to its orientation as well as its relatively higher (vertical) tilt angle. Second, the masking of PV panels for the diffused PAR_r strongly reduces for *N/S* schemes due to their smaller tilt angles. This is most prominent in mono-*N/S* due to its smallest tilt angle for which only 16% of *PAR* is transmitted to the ground at very high density of panels (*p/h* ≈ 1). These trends illustrate a tradeoff between PV energy and PAR_r. The seasonal PV energy production and PAR_r for the *N/S*- and *E/W*-faced schemes are shown in Figs. 6 and 7, respectively, for varying panel density. The seasonal PV energy trends for *E/W* and *N/S* schemes are similar and follow the expected variation in solar irradiation intensity across the seasons. The PAR_r values for *bi-E/W* PV are slightly higher relative to the *mono-N/S* in general for all panel densities. This trend becomes more significant for winter seasons and for high panel density.

1) Energy Yields and Land Productivity Factor: The annual energy yield and *LPF* [as defined in (*16*)] are shown in Fig. 8 for *bi-E/W* and *mono(bi)-N/S* PV as a function of the panel density. The energy yield for *bi-E/W* suffers due to mutual shading as *p/h* is significantly decreased as already discussed, which also results in a relatively higher PAR_r. At the half density (*p/h* ≈ 4), *LPF* is ∼1.35 and is not significantly different between *N/S*- and *E/W*-faced schemes. The *LPF*, however, drops for *bi-E/W* as the panel density is increased above the half density. At full density, the *LPF* ranges around 1.5–1.6 with *N/S*-faced panels providing slightly higher productivity.

B. Effect of the Tilt Angle

For fixed-tilt *N/S*-faced solar panels PV arrays at locations in the northern hemisphere, the PV tilt angle that is optimized for annual energy yield is known to be somewhat closer to the latitude of the location [23], [37], [38], whereas the monthly optimal PV tilt angle for energy yield is known to decrease from winter to summer months. For AV systems, the optimal tilt angle has to be adjusted according to the desired tradeoff for the sunlight sharing between panels and crops. Fig. 9 shows that the annual energy yield drops by 10 to 16% as the tilt angle varies from 20° to 60° for mono and bi-N/S PV schemes, respectively, at *p/h* = *2*. The annual PAR_r, on the other hand,

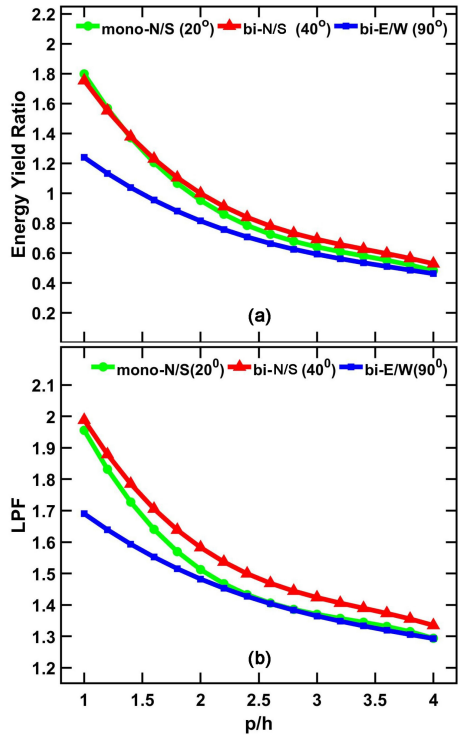

Fig. 8. (a) Energy yield ratio, and (b) *LPF* as a function of *p/h* for (*bi-E/W*) and (*mono-N/S* and *bi-N/S*) PV configurations.

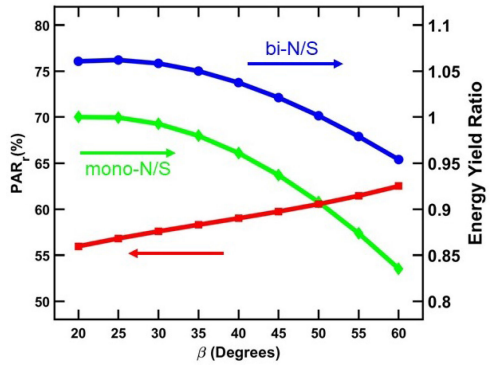

Fig. 9. Energy yield ratio and PAR_r as a function of the tilt angle.

shows a respective increase of ∼13% for the same variation in the *N/S* tilt angle. This shows that the tilt angle adjustment can be a useful knob to fine tune the required balance of PV/PAR_r once the system has been installed at a certain array density.

C. Optimal PV Array Density for Given Food–Energy Requirements

The design of an optimal array density for AV depends on system's food–energy requirements. Since there is a tradeoff between the relative food and energy production as the panel density is varied, therefore, an optimal array density is needed to provide the best balance between PV output and *PAR* reaching to the crops. Here, we assume a couple of AV design scenarios and explore optimal array topologies for these.

1) 80% *PAR* scenario, here, we optimize the array density ensuring that at least 80% of the *PAR* is transmitted to the ground relative to the open Sun condition.

TABLE I
SUMMARY OF OPTIMAL ARRAY DESIGN FOR BI-E/W AND MONO(BI)-N/S PV CONFIGURATIONS ENSURING ≥80% PAR_r YIELD

PV Scheme	p/h, (80% PAR_r Yield)	PV Energy Yield	LPF
mono-N/S	3.9	0.50	1.3
bi-N/S	3.9	0.55	1.35
bi-E/W	3.5	0.53	1.33

TABLE II
SUMMARY OF OPTIMAL ARRAY DESIGN FOR *BI-E/W* AND *MONO(BI)-N/S* PV CONFIGURATIONS ENSURING 80% ENERGY YIELD

PV Scheme	p/h, (80% PV Energy Yield)	PAR_r Yield	LPF
mono-N/S	2.6	0.62	1.42
bi-N/S	2.5	0.63	1.43
bi-E/W	2.1	0.67	1.47

2) 80% energy scenario, here, we optimize the array density that ensures 80% of the PV energy yield is obtained relative to the full density *mono-N/S* PV system.

Tables I and II show the required PV density and the respective *LPF* obtained for these designs, respectively. Table I shows that the optimal PV array density to implement 80% *PAR* scenario requires $p/h \approx 4$ for all three schemes. On the other hand, the required PV array density to implement 80% energy scenario is close to $p/h \approx 2.6$ and $p/h \approx 2$ for *N/S* and *bi-E/W* PV schemes, respectively. This relatively higher array density for 80% energy scenario design results in a drop of PAR_r to 60–70%.

IV. SUMMARY AND CONCLUSION

In this study, the relative effectiveness of the fixed-tilt vertical bifacial *E/W*-faced PV array for the first time for AV has been explored. A rigorous analytical framework has been developed to precisely calculate the sunlight intercepted by elevated PV arrays and the transmitted PAR below the elevated PV array. The following have been concluded.

1) Relative yields for PV energy and PAR_r have been similar for the vertical *bi-E/W* PV and *mono(bi)-N/S* PV when the panel density was half or lower relative to that of the standard ground-mounted PV farms. For denser PV arrays, *bi-E/W* has resulted in a higher crop yield at the cost of reduced energy yield. The relative PAR_r yield for *bi-E/W* increased as compared with *N/S* schemes when the array density was increased.
2) For PV arrays closer to the full density, the annual PAR_r dropped to 55–65%, while the relative PV yield for the vertical *bi-E/W* dropped to 80% with *LPF* close to 1.5.
3) For half density PV arrays, the annual PAR_r of ∼80% has been obtained, while the relative annual PV yields for vertical *bi-E/W* and *mono(bi)-N/S* PV dropped to 50–55% with *LPF* of 1.3–1.35.
4) For *N/S*-tilted PV schemes, adjustments in the tilt angle could enable fine tuning of the sunlight balance needed between PV and PAR_r. A modulation capability of 10–15% has been calculated while varying the N/S tilt angle between 20° and 60°.

5) The land productivity estimates for *mono(bi)-N/S*-tilted and *bi-E/W* vertical *E/W*-faced panels were although not significantly different for PV arrays that had half ($p/h = 4$) or lower density, some unique benefits for the *bi-E/W* vertical PV including minimal PV soiling (hence, better generation efficiency), minimal obstruction to rainfall and farm machinery, small land coverage, and possibly lower elevation requirements could make vertical *bi-E/W* AV farms preferable, especially for hot and arid climates having significant PV soiling concerns.
6) Finally, the economic factors that were deemed beyond the scope for this study should be considered to determine the ultimate choice of the preferable PV scheme for a particular AV application. In particular, since the bifacial solar panels can be somewhat more expensive, the capital cost for the bifacial system could be relatively higher. The vertical panels, on the other hand, could have a significantly lower cleaning requirement particularly for soiling intense environments. The relative levelized cost of energy should, therefore, be carefully evaluated considering the tradeoff between a higher capital cost versus low cost for periodic cleaning.

APPENDIX
SUPPLEMENTARY INFORMATION

A1 Model Validation

The global horizontal irradiation (*GHI*) and the PV energy output calculated using our model are compared with the experimental measurements in a reported AV field study at Montpellier, France [14]. *GHI* measurement data across the range of 16 days and PV energy output data for a sunny and cloudy day match well with the model output for the same location as shown in Figs. A1 and A2 respectively implying a good validity for our model.

A2 Effect of Temperature on PV Energy Output

An empirical model developed by King *et al.* [40] at Sandia National lab has been used to quantify the temperature effect for PV energy output. The module temperature is related to the ambient temperature (T_{amb}), incident irradiation (E), and wind speed (S_{wind}) by [40]:

$$T_{\mathrm{M}} = E \times e^{a+b\cdot S_{\mathrm{wind}}} + T_{\mathrm{amb}} \tag{17}$$

where a and b are the empirical constants. The temperature corrected efficiency η_{T} of the PV cell is then related to the standard cell efficiency η_{STC}:

$$\eta_{\mathrm{T}} = \eta_{\mathrm{STC}}[1 - T_{\mathrm{c}}\Delta T] \tag{18}$$

where (T_{c}) is the temperature coefficient (assumed to be 0.41%/°C [41] for crystalline silicon panels) and ΔT is the difference in the ambient and cell temperatures.

A3 Effect of Bypass Diode

The power-output estimate in our model is an optimistic upper bound which incorporates mutual shading of the direct light as an irradiance loss but does not incorporate the practical module configuration that involves bypass diodes. To estimate the difference, we compare the power outputs of our model with that from [31] which does include the practical module configuration with 3 bypass diodes. The daily power outputs of solar farm calculated from the two models are shown in Fig. A4 assuming E/W facing vertical bifacial module arrays for a particular day (Sep 22) at Washington DC. The two models converge as the array density is lowered ($p/h > 2.5$). The

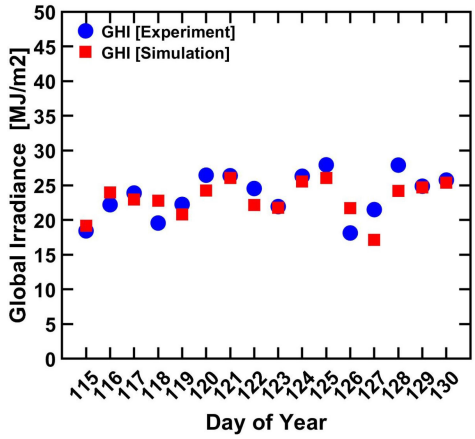

Fig. A1. Global horizontal irradiation from the model output vs. measured field data [14]

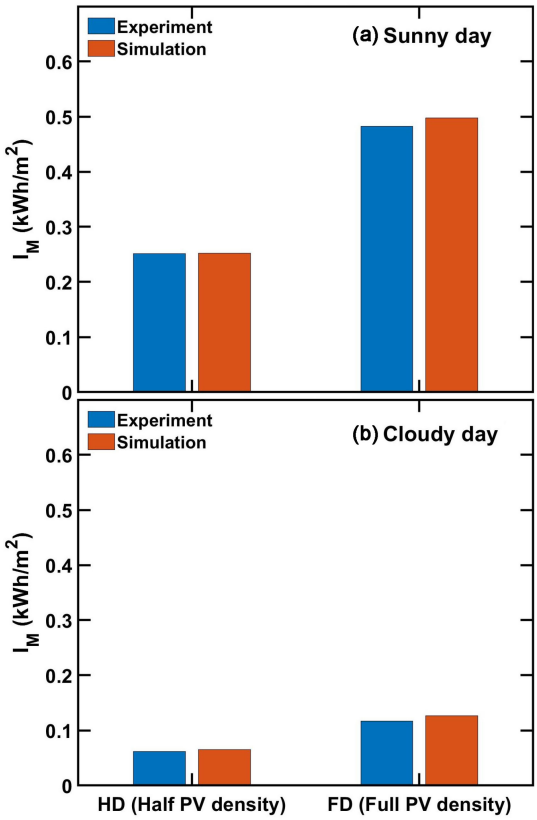

Fig. A2. PV energy output comparison between our model and measured field data [39] for a sunny and cloudy day.

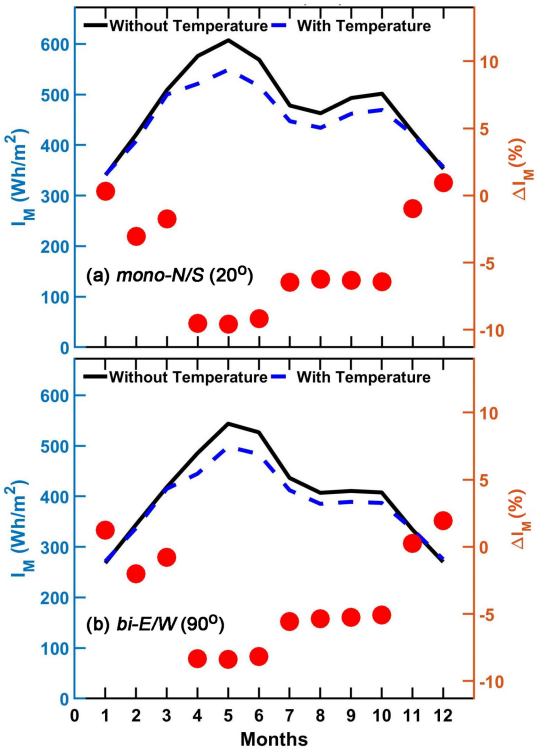

Fig. A3. PV energy output for each month with and without the temperature effect for (left) mono-N/S and (right) bi-E/W PV schemes. The percentage difference in the PV output due to the temperature effect is also shown (circles).

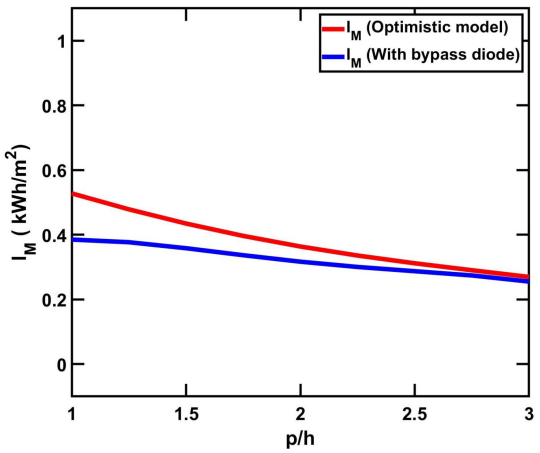

Fig. A4. Comparison of the power outputs of our model with that from [31] which includes the practical module configuration with 3 bypass diodes.

difference is however significant (∼30%) for extremely dense array ($p/h = 1$). For N/S faced arrays, one expects a similar trend. From this discussion, we conclude that the relative output power trends between the E/W and N/S configurations (see Fig. 6) are reasonably accurate for $p/h \geq 2$. For agrivoltaic applications, the array density is typically lower (*i.e.* $p/h > 2$), suggesting that the effect is relatively small. Future research on the topic should however incorporate practical cell configuration on the module in model to precisely quantify mutual shading effect.

ACKNOWLEDGMENT

The authors would like to thank the doctoral students' support and high performance computing resources by the Lahore University of Management Science.

REFERENCES

[1] A. Goetzberger and A. Zastrow, "On the coexistence of solar-energy conversion and plant cultivation," *Int. J. Sol. Energy*, vol. 1, no. 1, pp. 55–69, 1982.
[2] H. Dinesh and J. M. Pearce, "The potential of agrivoltaic systems," *Renewable Sustain. Energy Rev.*, vol. 54, pp. 299–308, 2016.
[3] A. Weselek *et al.*, "Agrophotovoltaic systems: Applications, challenges, and opportunities. A review," *Agronomy Sustain. Develop.*, vol. 39, no. 4, p. 35, 2019.
[4] R. Mead and R. Willey, "The concept of a 'land equivalent ratio' and advantages in yields from intercropping," *Exp. Agriculture*, vol. 16, no. 3, pp. 217–228, 1980.
[5] Y. Elamri, B. Cheviron, J.-M. Lopez, C. Dejean, and G. Belaud, "Water budget and crop modelling for agrivoltaic systems: Application to irrigated lettuces," *Agricultural Water Manage.*, vol. 208, pp. 440–453, 2018.
[6] E. Gençer *et al.*, "Directing solar photons to sustainably meet food, energy, and water needs," *Sci. Rep.*, vol. 7, no. 1, pp. 1–7, 2017.
[7] S. Parkinson and J. Hunt, "Economic potential for rainfed agrivoltaics in groundwater-stressed regions," *Environ. Sci. Technol. Lett.*, 2020.
[8] S. Schindele *et al.*, "Implementation of agrophotovoltaics: Techno-economic analysis of the price-performance ratio and its policy implications," *Appl. Energy*, vol. 265, 2020, Art. no. 114737.
[9] E. H. Adeh, J. S. Selker, and C. W. Higgins, "Remarkable agrivoltaic influence on soil moisture, micrometeorology and water-use efficiency," *PLoS One*, vol. 13, no. 11, 2018, Art. no. e0203256.
[10] D. Majumdar and M. J. Pasqualetti, "Dual use of agricultural land: Introducing 'agrivoltaics' in phoenix metropolitan statistical area, USA," *Landscape Urban Planning*, vol. 170, pp. 150–168, 2018.
[11] G. A. Barron-Gafford *et al.*, "Agrivoltaics provide mutual benefits across the food-energy-water nexus in drylands," *Nat. Sustain.*, vol. 2, pp. 848–855, 2019.
[12] C. Dupraz *et al.*, "Combining solar photovoltaic panels and food crops for optimising land use: Towards new agrivoltaic schemes," *Renewable Energy*, vol. 36, no. 10, pp. 2725–2732, 2011.
[13] C. Dupraz *et al.*, "To mix or not to mix: Evidences for the unexpected high productivity of new complex agrivoltaic and agroforestry systems," in *Proc. 5th World Congr. Conservation Agriculture, Resilient Food Syst. Changing World*, 2011.
[14] H. Marrou, L. Guilioni, L. Dufour, C. Dupraz, and J. Wèry, "Microclimate under agrivoltaic systems: Is crop growth rate affected in the partial shade of solar panels?," *Agricultural Forest Meteorol.*, vol. 177, pp. 117–132, 2013.
[15] P. R. Malu, U. S. Sharma, and J. M. Pearce, "Agrivoltaic potential on grape farms in India," *Sustain. Energy Technol. Assessments*, vol. 23, pp. 104–110, 2017.
[16] S. Amaducci, X. Yin, and M. Colauzzi, "Agrivoltaic systems to optimise land use for electric energy production,"*Appl. Energy*, vol. 220, pp. 545–561, 2018.
[17] T. Sekiyama and A. Nagashima, "Solar sharing for both food and clean energy production: Performance of agrivoltaic systems for corn, a typical shade-intolerant crop,"*Environments*, vol. 6, no. 6, p. 65, 2019.
[18] M. T. Patel *et al.*, "Temperature dependent energy gain of bifacial PV farms: A global perspective," 2020, *arXiv:2003.03660*.
[19] C. D. Rodrìguez-Gallegos *et al.*, "Monofacial vs bifacial Si-based PV modules: Which one is more cost-effective?," *Sol. Energy*, vol. 176, pp. 412–438, 2018.
[20] C. D. Rodrìguez-Gallegos *et al.*, "Global techno-economic performance of bifacial and tracking photovoltaic systems," *Joule*, vol. 4, pp. 1514–1541, 2020.
[21] S. Guo, T. M. Walsh, and M. Peters, "Vertically mounted bifacial photovoltaic modules: A global analysis," *Energy*, vol. 61, pp. 447–454, 2013.
[22] D. Chudinzow, S. Nagel, J. Güsewell, and L. Eltrop, "Vertical bifacial photovoltaics—A complementary technology for the European electricity supply?," *Appl. Energy*, vol. 264, 2020, Art. no. 114782.
[23] A. Ullah, H. Imran, Z. Maqsood, and N. Z. Butt, "Investigation of optimal tilt angles and effects of soiling on PV energy production in Pakistan," *Renewable Energy*, vol. 139, pp. 830–843, 2019.

[24] A. A. Hegazy, "Effect of dust accumulation on solar transmittance through glass covers of plate-type collectors," *Renewable Energy*, vol. 22, no. 4, pp. 525–540, 2001.
[25] A. M. Al-Sabounchi, S. A. Yalyali, and H. A. Al-Thani, "Design and performance evaluation of a photovoltaic grid-connected system in hot weather conditions," *Renewable Energy*, vol. 53, pp. 71–78, 2013.
[26] M. T. Patel, M. R. Khan, X. Sun, and M. A. Alam, "A worldwide cost-based design and optimization of tilted bifacial solar farms," *Appl. Energy*, vol. 247, pp. 467–479, 2019.
[27] I. Reda and A. Andreas, "Solar position algorithm for solar radiation applications," *Sol. Energy*, vol. 76, no. 5, pp. 577–589, 2004.
[28] *PV Performance Modeling Collaborative*: *An Industry and National Laboratory Collaborative to Improve Photovoltaic Performance Modeling*. 2016. Accessed: Sep. 19, 2019. [Online]. Available: https://pvpmc.sandia.gov/
[29] B. Haurwitz, "Insolation in relation to cloudiness and cloud density," *J. Meteorol.*, vol. 2, no. 3, pp. 154–166, 1945.
[30] *Power Surface Meteorology and Solar Energy: A Renewable Energy Resource Web Site* (release 6.0), 2017. [Online]. Available: https://eosweb.larc.nasa.gov/cgi-bin/sse/sse.cgi?/
[31] M. R. Khan, A. Hanna, X. Sun, and M. A. Alam, "Vertical bifacial solar farms: Physics, design, and global optimization," *Appl. Energy*, vol. 206, pp. 240–248, 2017.
[32] M. H. Riaz, H. Imran, and N. Z. Butt, "Optimization of PV array density for fixed tilt bifacial solar panels for efficient agrivoltaic systems," in *Proc. IEEE 47th Photovolt. Spec. Conf.*, 2020, pp. 1349–1352.
[33] H. Imran, M. H. Riaz, and N. Z. Butt, "Optimization of single-axis tracking of photovoltaic modules for agrivoltaic systems," in *Proc. IEEE 47th Photovolt. Spec. Conf.*, 2020, pp. 1353–1356.
[34] K. R. McIntosh *et al.*, "An optical comparison of silicone and EVA encapsulants for conventional silicon PV modules: A ray-tracing study," in *Proc. 34th IEEE Photovolt. Spec. Conf.*, 2009, pp. 544–549.
[35] K. R. McIntosh, J. N. Cotsell, A. W. Norris, N. E. Powell, and B. M. Ketola, "An optical comparison of silicone and EVA encapsulants under various spectra," in *Proc. 35th IEEE Photovolt. Spec. Conf.*, 2010, pp. 269–274.
[36] H. Imran, Z. Maqsood, A. Ullah, and N. Z. Butt, "Effective prediction of transmission of solar irradiance through dusty solar panels using atmospheric aerosol data for Lahore, Pakistan," in *Proc. IEEE 46th Photovolt. Spec. Conf.*, 2019, pp. 2889–2893.
[37] T. O. Kaddoura, M. A. Ramli, and Y. A. Al-Turki, "On the estimation of the optimum tilt angle of PV panel in Saudi Arabia," *Renewable Sustain. Energy Rev.*, vol. 65, pp. 626–634, 2016.
[38] H. Khorasanizadeh, K. Mohammadi, and A. Mostafaeipour, "Establishing a diffuse solar radiation model for determining the optimum tilt angle of solar surfaces in Tabass, Iran," *Energy Convers. Manage.*, vol. 78, pp. 805–814, 2014.
[39] B. Valle *et al.*, "Increasing the total productivity of a land by combining mobile photovoltaic panels and food crops,"*Appl. Energy*, vol. 206, pp. 1495–1507, 2017.
[40] D. L. King, J. A. Kratochvil, and W. E. Boyson, *Photovoltaic Array Performance Model*, US Dept. Energy, Oak Ridge, TN, USA, 2004, pp. 1–43.
[41] PV Education Website. Accessed: Jan. 12, 2021. [Online]. Available: https://www.pveducation.org/pvcdrom/solar-cell-operation/effect-of-temp%erature/